2023

Advanced Microstructural Characterization of Functionally Graded Dental Ceramic Material for Materials-Informed Finishing

Angani Vigneswaran
University of Kentucky, avi230@uky.edu
Digital Object Identifier: https://doi.org/10.13023/etd.2023.362

STUDENT AGREEMENT:

I represent that my thesis or dissertation and abstract are my original work. Proper attribution has been given to all outside sources. I understand that I am solely responsible for obtaining any needed copyright permissions. I have obtained needed written permission statement(s) from the owner(s) of each third-party copyrighted matter to be included in my work, allowing electronic distribution (if such use is not permitted by the fair use doctrine) which will be submitted to UKnowledge as Additional File.

I hereby grant to The University of Kentucky and its agents the irrevocable, non-exclusive, and royalty-free license to archive and make accessible my work in whole or in part in all forms of media, now or hereafter known. I agree that the document mentioned above may be made available immediately for worldwide access unless an embargo applies.

I retain all other ownership rights to the copyright of my work. I also retain the right to use in future works (such as articles or books) all or part of my work. I understand that I am free to register the copyright to my work.

REVIEW, APPROVAL AND ACCEPTANCE

The document mentioned above has been reviewed and accepted by the student's advisor, on behalf of the advisory committee, and by the Director of Graduate Studies (DGS), on behalf of the program; we verify that this is the final, approved version of the student's thesis including all changes required by the advisory committee. The undersigned agree to abide by the statements above.

Angani Vigneswaran, Student

Dr. Julius M. Schoop, Major Professor

Dr. Fazleena Badurdeen, Director of Graduate Studies

ADVANCED MICROSTRUCTURAL CHARACTERIZATION OF FUNCTIONALLY GRADED DENTAL CERAMIC MATERIAL FOR MATERIALS-INFORMED FINISHING

THESIS

A thesis submitted in partial fulfillment of the
requirements for the degree of Master of Science in
Manufacturing Systems Engineering in the
College of Engineering at the University of Kentucky

By

Angani Vigneswaran

Elk Grove, California

Director: Dr. Julius M. Schoop, Professor of Mechanical Engineering

Lexington, Kentucky

2023

ABSTRACT OF THESIS

ADVANCED MICROSTRUCTURAL CHARACTERIZATION OF FUNCTIONALLY GRADED DENTAL CERAMIC MATERIAL FOR MATERIALS-INFORMED FINISHING

Yttria-stabilized tetragonal zirconia polycrystal (Y-TZP) has gained popularity as the choice of material for dental prosthetics. Ivoclar Vivadent's IPS e.max ZirCAD Prime dental ceramic incorporates a unique gradient technology that varies the yttria content over the thickness of the material. The top layer is composed of 5Y-TZP which is desired for its optical properties while the bottom layer is composed of a much stronger 3Y-TZP. In between the two layers, 5Y-TZP and 3Y-TZP are mixed to form a transition layer. Varying the amount of yttria allows for more esthetically pleasing translucency in the visible areas of the restoration without compromising mechanical strength in the body. This study aims to address the gap between microstructural characterization of this dental ceramic and machining parameters that are relevant to the dental professionals performing surface finishing.

The material was examined, before and after sintering, via scanning electron microscopy (SEM), electron backscatter diffraction (EBSD), and energy-dispersive X-ray spectroscopy (EDS), from which average grain size, crystallographic orientation, and elemental composition were analyzed. Critical linear feed rates were derived from these measured parameters. The recommendation of using high cutting speeds addresses the variability in linear feed rate of handheld finishing tools as well as the ductile-to-brittle transition of IPS e.max ZirCAD Prime.

KEYWORDS: Dental Ceramic, Yttria-Stabilized Zirconia, Gradient Technology, Microstructural Characterization, Ductile Machining, Surface Finishing

Angani Vigneswaran

08/10/2023

Date

ADVANCED MICROSTRUCTURAL CHARACTERIZATION OF FUNCTIONALLY GRADED DENTAL CERAMIC MATERIAL FOR MATERIALS-INFORMED FINISHING

By
Angani Vigneswaran

Dr. Julius M. Schoop
Director of Thesis

Dr. Fazleena Badurdeen
Director of Graduate Studies

08/10/2023
Date

ACKNOWLEDGMENTS

I would like to express my sincere gratitude to my advisor, Dr. Julius M. Schoop, for his endless guidance, patience, and support. His wisdom and dedication were essential for the completion of this project. I thank him for providing me with this valuable learning opportunity.

I would like to extend my gratitude to Dr. Howard W. Roberts, the co-PI of this project. His expertise, along with his inspiring enthusiasm, were critical for completing the project in a timely manner.

I wish to thank my committee members, Dr. Fazleena Badurdeen and Dr. Ibrahim S. Jawahir, for their time and guidance, not only during my research project, but also throughout the course of my master's program.

This project was supported by grant P20GM103436 (KY INBRE) from the National Institute of General Medical Sciences, National Institutes of Health. I would like to thank Kentucky IDeA Networks of Biomedical Research Excellence for their generous support in funding the sample preparation and use of electron microscopy. A big thank you to Nicolas J. Briot and Avery Hartley for the time they invested in obtaining and providing the experimental data.

Last but certainly not least, I would like to thank my family for their unwavering support and encouragement. Thank you Appa and Amma for always pushing me to strive for the best. You lead by example that with hard work, anything is possible. Anu, thank you for being my thambi.

TABLE OF CONTENTS

LIST OF TABLES

LIST OF FIGURES

CHAPTER 1. INTRODUCTION

Whether it be due to disease or injury, the various parts of the human body are susceptible to impairment, impacting health and quality of life. A chipped tooth, for example, could be debilitating, but that does not have to be the case necessarily. Evidence shows that throughout the history of humankind innovative solutions have been developed to mitigate or remediate medical conditions. Naturally occurring materials have been engineered to enhance or replace biological tissue. Now, advancements in medicine and engineering have made it possible for synthetic substances to be used as biomaterials.

Prosthodontic treatments in restorative dentistry provide patients with artificial teeth to ameliorate their oral health and daily functions, importantly mastication. There is also the added cosmetic benefit of an improved smile. Restorative dental materials have evolved with the emergence of new technologies and methods. Egyptian mummies were found with ivory, wood, and various metals in their mouths (Johnson, 1959). During the 18th century, great progress was made in prosthodontics, thanks to the works of Pierre Fauchard (known as “the founder of modern dentistry” and “the father of modern dental prosthesis”), Claude Monton, and Etienne Bourdet (Johnson, 1959). They experimented with teeth from human and animal sources, ivory, porcelain, and metals (Johnson, 1959). Fast forward to recent times and the choice of material for dental crowns include metallic alloys, porcelain fused to metal, resin, and ceramics (Sakaguchi et al., 2019). Selecting the optimal material requires consideration of a wide range of factors, from biocompatibility to mechanical strength to manufacturability. Each type of material will inherently present certain advantages and disadvantages, but the decision comes down to striking the right balance. In this sense, there has been a shift away from metals and towards high strength

ceramics, which have become quite reputable for their esthetic and chemical inertness as well as favorable mechanical properties (Stawarczyk et al., 2017).

1.1 Structure & Properties of Polymorphic Zirconia

Zirconium dioxide (ZrO_2), also called zirconia, has gained popularity as a dental ceramic over the last few decades. At different temperatures, zirconia can exist in one of three crystalline configurations: monoclinic, tetragonal, and cubic (Figure 1.1). At room temperature, zirconia is stable in the monoclinic phase. At 1170ºC, there is a phase transformation to the tetragonal phase that is accompanied by an approximate 4-5% volume decrease. Finally, above 2370ºC, the cubic phase is predominant, with little to no volume change (Kisi & Howard, 1998). During cooling, the reverse martensitic transformation from the tetragonal to the monoclinic phase ($t \rightarrow m$) is characterized by a 4-5% volume increase. The sudden volume increase renders the use of pure zirconia for dental applications unattainable as the elevated internal tension results in cracks and defects (Piconi & Maccauro, 1999; Stawarczyk et al., 2017). However, the $t \rightarrow m$ transformation during cooling can be prevented by doping zirconia with stabilizing oxides such as CaO, MgO, CeO_2, and Y_2O_3 (Denry & Kelly, 2007).

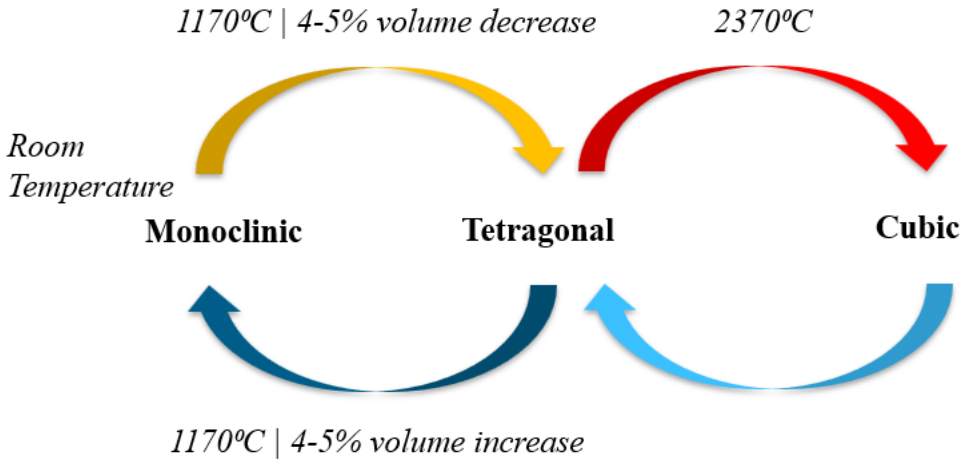

Figure 1.1 The phase transformations of zirconia at different temperatures.

The most commonly used stabilizer in dentistry is yttrium oxide, or yttria (Y_2O_3) (Soleimani et al., 2020). This stabilized zirconia material is called tetragonal polycrystalline zirconia (TPZ) or tetragonal zirconia polycrystal (TZP). The monoclinic phase is disfavored, and the cubic and tetragonal phases exist in varying amounts as metastable phases at room temperature (Singhal, 2020). The first dental zirconia mainstay was the addition of 3 mol% yttria, known as 3 mol% yttria tetragonal zirconia polycrystal (3Y-TZP) (Zhang & Lawn, 2019). 3Y-TZP is composed of 80 wt% tetragonal phase and 20 wt% cubic phase, and its enhanced mechanical properties are attributed to a transformation toughening phenomenon (Zhang et al., 2020). When a crack forms and begins to propagate, its large tensile stresses alleviate the constraints of the matrix. This induces a local phase transformation from the tetragonal phase to the monoclinic phase. The associated volume expansion compresses the crack and prevents it from further propagating (Garvie et al., 1975; Pelleg, 2014).

3Y-TZP possesses the highest strength and toughness of all dental ceramics (Chevalier & Gremillard, 2017; Ali et al., 2014). But it is lacking in its optical properties - its opacity is not as esthetically pleasing for those who would prefer the restoration to resemble natural teeth. To enhance translucency and create more teeth-like shades, the yttria concentration has been increased to 4 mol% and 5 mol% yttria (4Y-TZP and 5Y-TZP, respectively), resulting in a composition of 40-70 wt% cubic phase (Zhang et al., 2020). The improved optical properties come at a cost. With the reduction in the amount of tetragonal phase, transformation toughening can no longer occur and there is a loss in mechanical performance (Zhang et al., 2020).

An attempt to remedy the loss of mechanical strength while maintaining improved esthetics has been recently introduced by using a multi-layered technique in which different yttria content is varied over a disc thickness, resulting in different amounts of the cubic phase in each layer (Vardhaman et al., 2020). This layering combination is mainly between a high-flexural strength 3Y-TZP in the dentin/body area for higher strength and a highly translucent 5Y-TZP that is placed in the more visible areas for better esthetics (Michailova et al., 2020).

1.2 IPS e.max ZirCAD Prime: A Functionally Graded Dental Ceramic

The material of interest for this study is the IPS e.max ZirCAD Prime (shade A2) from Ivoclar Vivadent. The manufacturer has incorporated gradient technology in which the top layer (incisal zone) is the more translucent 5Y-TZP layer, the transition zone is a mix of 5Y- and 3Y-TZP, and the bottom dentin zone consists of the stronger 3Y-TZP, as shown in Figure 1.2.

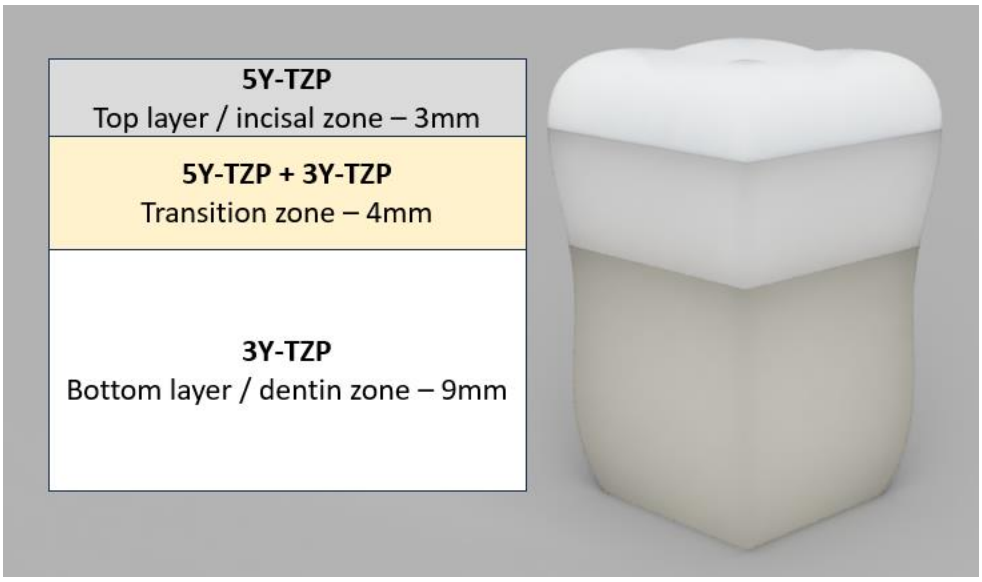

Figure 1.2 An illustration depicting the gradient composition of IPS e.max ZirCAD Prime (Ivoclar Vivadent).

The introduction of CAD/CAM (computer-aided design/computer-aided manufacturing) has allowed dentists to scan the patient's mouth, create a restoration, and implant it, all within a day's time (Skorulska et al., 2021). Ivoclar Vivadent has produced this ceramic with the intention of dental practitioners using CAD/CAM to create the final restoration. The procedure to convert the disc of material to the desired crown or bridge includes the following steps: CAD design, CAM nesting, milling, finishing, sintering, finishing, and staining/glazing (Ivoclar Vivadent). Ivoclar Vivadent recommends fine tungsten carbide burs and diamond grinding instruments for separating and finishing the pre-sintered restorations. Fine diamond grinding instruments and rubber polishers are recommended for post-sintered processing.

Due to the advertised layered process, the restoration must be prepared to optimize the different layers contained in the disc. Furthermore, the additional steps of finishing require careful selection of tools and machining parameters to minimize the risk of damage and early failure of the restoration. Through characterization, a clearer understanding of the microstructure is made possible, both in the pre- and post-sintered states, which then help to provide finishing recommendations for the improved performance of the IPS e.max ZirCAD Prime dental ceramic.

CHAPTER 2. LITERATURE REVIEW

2.1 Significance of Characterizing the Microstructure

Grain size and microstructure play a crucial role in determining the physical properties and performance of materials. Grain size refers to the average size of individual grains within a material's microstructure while microstructure encompasses the arrangement, distribution, and characteristics of these grains as well as other constituents such as pores. Pelleg (2014) describes grains and grain boundaries as dislocation inhibitors. The Hall-Petch relationship (shown by the equation below) describes the influence of grain size on the strength of crystalline materials. It states that the strength of a material increases as the average grain size decreases (Pelleg, 2014; Trunec, 2008).

$$\sigma = \sigma_0 + k_1 d^{-0.5}$$

where:

- σ is the yield strength of the material.
- σ_0 is a material-specific constant representing the strength contribution from mechanisms other than grain size (such as solid solution strengthening or precipitate strengthening).
- k_1 is the Hall-Petch coefficient, which reflects the strength increase per unit reduction in grain size.
- d is the average grain size of the material.

The presence of grain boundaries, which are the interfaces between adjacent grains, can impede dislocation motion and hinder deformation. As the grain size decreases, the number of grain boundaries increases, creating more obstacles for dislocations to move and interact. This results in a greater resistance to deformation and an increase in the material's strength (Pelleg, 2014). But it must be noted that the Hall-Patch relationship only holds true in the submicron range (Trunec, 2008; Eichler et al., 2007). Nanocrystalline materials (< 100 nm) deviate from this relationship since their fracture toughness depends on the grain size itself. In addition to grain size, polycrystalline ceramics can exhibit anisotropy, a “directionally-dependent property” (Pelleg, 2014). Isotropic materials have consistent properties in whichever crystal orientation, whereas anisotropic materials have texture, or a preferred orientation, that can affect physical properties in those directions.

2.2 Microstructural Characterization of IPS e.max ZirCAD Prime

While different types and brands of 3Y-TZP and 5Y-TZP dental applications have been investigated, there is limited research on the characterization of ZirCAD Prime specifically and, thus, limited information on finishing recommendations that can be provided to professionals in the dental industry.

Inokoshi et al. (2023) performed X-ray diffraction (XRD) analysis which revealed that the top and bottom layers consist of 51.32 wt% and 18.11 wt% of the cubic phase, respectively, while in the transition layer it varied between 34.23 wt% and 51.19 wt%. X-ray fluorescence spectroscopy (XRF) determined the content of Y_2O_3 to be 5.6 mol% in the top layer, mix of 3.86 mol% and 4.69 mol% in the middle layer, and 3.1 mol% in the

bottom layer. Scanning electron microscopy (SEM) was used to calculate grain sizes and the observation made was that grain size decreases from the top to bottom layer, with the bottom layer having the smallest grain size. It was also observed that the middle transition layer had the greatest variation in grain size.

Strasser et al. (2023) came to a similar conclusion with their SEM analysis and XRD analysis confirmed that the top, middle, and bottom layers consisted of 5Y-TZP, mixture of 5Y-TZP and 3Y-TZP, and 3Y-TZP, respectively.

Dimitriadis et al. (2023) performed thermal etching after SEM and measured the grain sizes to be 1130 ± 490, 900 ± 190, and 340 ± 110 nm, in the top, middle, and bottom layers, respectively.

Marini et al. (2023) reported grain size measurements from SEM of less than 0.50 μm in all layers, without no statistical difference between the three.

Winter et al. (2022) conducted energy-dispersive X-ray spectroscopy (EDX) to find that the highest yttria content is in the top layer and decreases down to the bottom layer. Their analysis also revealed the presence of lanthanum along with the expected zirconium, yttrium, oxygen, aluminum, and hafnium.

Rosentritt et al. (2020) found via SEM that the top layer contained grains measuring around 1 μm and grains in the remaining layers measured around half the size. They also observed that the bottom layer grains were slightly larger than those in the middle layer.

2.3 Finishing Parameters

Finishing refers to the machining process in which the surface of a workpiece is refined, polished, or improved to achieve the desired appearance, dimensional accuracy, and surface quality. It involves removing any remaining imperfections, roughness, or tool marks left from earlier manufacturing operations. Depending on the specific requirements of the application, finishing can involve various techniques and processes specific to the desired outcome (Schey, 2009). Finishing processes involve various parameters that are carefully controlled to achieve the desired product. The specific parameters depend on the type of finishing process and the material being worked on. Schey (2009) mentions the following as common parameters in finishing processes:

- Cutting Speed: The speed at which the tool or workpiece moves relative to each other during the finishing operation. It influences the material removal rate, surface finish, and tool life.
- Feed Rate: The rate at which the tool or workpiece advances per unit of time. It affects the material removal rate, surface roughness, and tool wear.
- Depth of Cut: The thickness or amount of material removed in a single pass. It influences the material removal rate, cutting forces, and surface finish.
- Tool Geometry: The shape, size, and cutting edge geometry of the tool. It impacts the chip formation, cutting forces, surface finish, and tool life.
- Tool Material: The material from which the tool is made. It determines the tool's wear resistance, toughness, and thermal properties, which affect its performance and tool life.

- Coolant or Lubricant: The use of coolants or lubricants during the finishing process to reduce heat, friction, and tool wear. It helps to control chip formation, improve surface finish, and extend tool life.

2.4 Ductile to Brittle Transition

In order to achieve good surface quality, precision machining is necessary. However, a ceramic's brittleness makes it prone to cracks and early fracture (Singh et al., 2020). This issue can be avoided by employing ductile mode machining (Choudhary & Paul, 2021; Bifano et al., 1991). Ductile removal consists of the chip deforming through rubbing, plowing, and chip formation (Sun et al., 2015). The workpiece undergoes a great amount of plastic deformation before fracturing. During brittle removal, there is fracture forming, fracture spreading, and peeling off, resulting in potential cracks and rough surfaces. The transition between ductile and brittle mode is influenced by the many machining parameters. But if the grinding depth is less than the ductile-brittle transition depth, then ductile removal will occur and smooth surfaces with minimal defects can be expected (Yang et al., 2019).

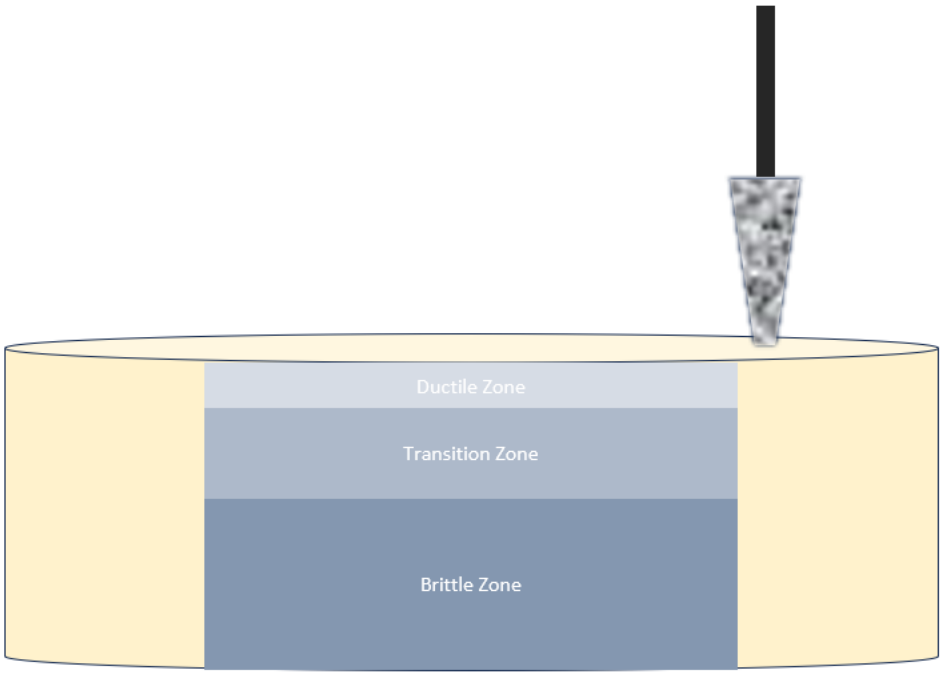

Figure 2.1 Illustration to depict varying grinding depths at which a tool can reach the ductile, transition, or brittle zone of a workpiece.

The grain size of a material is a critical factor in machining as it directly affects the material's mechanical properties and response to cutting forces (Yang et al., 2020; Armstrong, 1970). According to the Hall-Petch relationship, finer grains exhibit higher strength and vice versa; this applies to both the workpiece and the tool. Careful consideration of available resources must be made to determine the optimal combination of machining parameters to achieve efficient material removal, desired surface finish, and extended tool life while ensuring the integrity of the workpiece.

CHAPTER 3. EXPERIMENTAL PROCEDURE

3.1 Background Information on SEM, EBSD, & EDS

In scanning electron microscopy (SEM), electrons are emitted and collimated into a beam. This beam travels through a set of electromagnetic lenses (in the electron column) that focus the beam onto the sample. Kinetic energy from the beam results in elastic and inelastic collisions with the sample atoms which then emit different kinds of signals, including backscattered electrons, secondary electrons, Auger electrons, x-rays, and cathodoluminescence. Backscattered electrons are electrons that are reflected back from the original electron beam and come from deep within a sample. They provide information on crystallography, topography, and magnetic field. Secondary electrons originate from the surface of the sample and are useful for examining topography. Auger electrons are ejected due to energy from an electron in one shell jumping into a vacancy in an inner shell. Information regarding elemental composition from the top surface is revealed through these particular electrons. X-rays that are produced when the electron beam hits the surface provide information about elemental composition as well. Finally, cathodoluminescence, emitted light, is used for image resolution (Datye & DeLaRiva, 2023).

Electron backscatter diffraction (EBSD) is a SEM-based technique in which an electron beam is scanned across a tilted crystalline sample. A diffraction pattern in produced from which the following information can be extracted: crystal structure and orientation as well as grain morphology and boundaries (Wilkinson & Britton, 2012).

Energy-dispersive X-ray spectroscopy (EDS) detects and analyzes the x-rays that are emitted during SEM in an energy spectrum. Energy peaks provide information on the elemental composition of the material (Hodoroaba, 2020).

3.2 Data Collection

A 1 cm x 1 cm block was cut and polished from the 16 mm thick IPS e.max ZirCAD Prime disc while it was in its green state as shown in Figure 3.1. Polishing was performed according to a 5-step process as shown in Table 3.1.

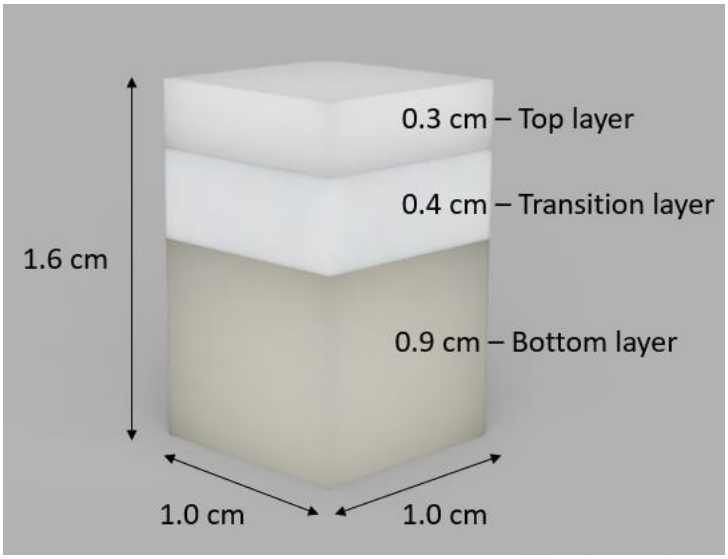

Figure 3.1 Diagram of the experimental sample of IPS e.max ZirCAD Prime.

Table 3.1 Steps for polishing the pre-sintered sample (Pace Technologies, n.d.).

Abrasive	Lubricant	Force	Speed (head/base)	Time
70 µm diamond grinding disk	Water	5-10 lbs	200/200 rpm	Planar
30 µm DIAMAT diamond suspension on CERMESH Metal Mesh cloth		5-10 lbs	200/200 rpm	5 min
6 µm DIAMAT diamond on TEXPAN polishing pad	SIAMAT colloidal silica	10 lbs	200/200 rpm	5 min
1 µm DIAMAT diamond on GOLDPAD or ATLANTIS polishing pad	SIAMAT colloidal silica	10 lbs	200/200 rpm	5 min
SIAMAT diamond on TEXPAN polishing pad		10 lbs	200/200 rpm	5 min

Scanning electron microscopy (SEM), electron backscatter diffraction (EBSD), and energy dispersive spectroscopy (EDS) were performed at various locations along the sample using the FEI Helios Nanolab 660 Dual Beam System (Electron Microscopy Center, University of Kentucky).

For post-sintering analysis, the same 1 cm x 1 cm x 16 mm sample was sintered using the Programat S1 (version 6.0) sintering furnace. The manufacturer's instructions were followed as shown in Table 3.2.

Table 3.2 Sintering program (Ivoclar Vivadent)

	Temperature 1 (ºC)	Temperature 2 (ºC)	Heating-up rate (ºC/min)	Dwell time (min)
Heating phase	20	900	10	-
Holding phase	900	900	-	30
Heating phase	900	1500	3.3	-
Holding phase	1500	1500	-	120
Cooling phase	1500	900	10	-
Cooling phase	900	300	8.3	-

Following sintering, the sample was mounted using a conductive copper compression mounting powder and polished according to Table 3.1.

Again, SEM, EBSD, and EDS were performed at various locations on the sample. ImageJ software was used to measure grain size in the SEM and EBSD images.

3.3 Statistical Analysis of Data

Minitab statistical software was used to analyze the data. Pre-sintered data indicated normal distribution. For the post-sintered measurements, outliers were removed after which the Anderson-Darling Normality Test was performed. For the top, transition, and bottom layers of the post-sintered sample, p-values of 0.326, 0.010, and 0.935 were calculated, respectively, indicating normal distribution for the top and bottom layers, but non-normal distribution for the transition layer. Johnson transformation was performed to normalize the dataset from the transition layer. Mood's median test was conducted and p-value of 0.000 was the result.

CHAPTER 4. RESULTS & DISCUSSION

4.1 Pre-Sintered Sample

Images of ZirCAD Prime in its green state reveal a quite porous microstructure composed of irregular and angular shaped particles. The average grain size was measured to be 0.102 µm with a standard deviation of 0.032 µm.

While more studies would need to be conducted, this material in its green state could potentially be categorized as a nanostructured ceramic (grain size <100 nm). Ceramics are known to be brittle, but nano-sized particles can allow for "superplastic deformation" (Mayo, 1996). In addition to high ductility, nanocrystalline materials also exhibit high strength and hardness, compared to the more coarse-grained materials (Pelleg, 2014; Mayo, 1996). The small size also promotes lower sintering temperature and times, resulting in high production rates at low costs (Arena et al., 2019).

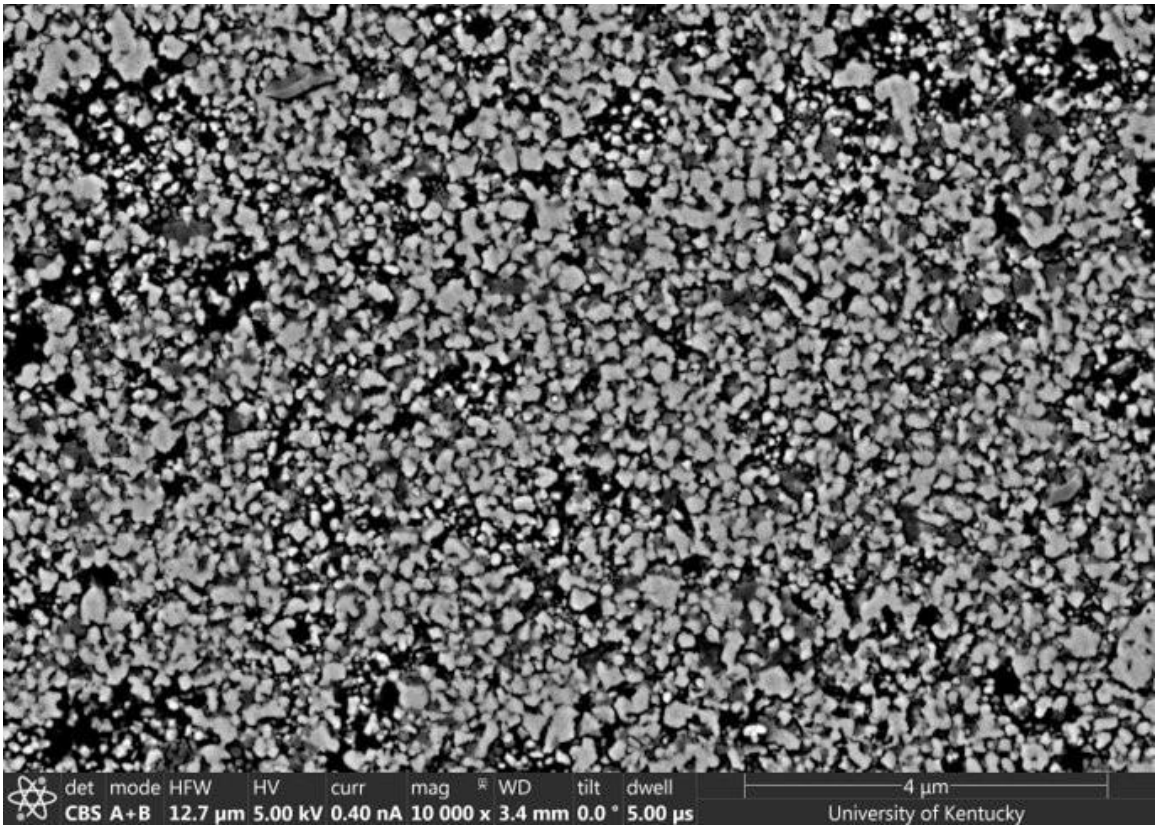

Figure 4.1 SEM image of the experimental sample in its green state.

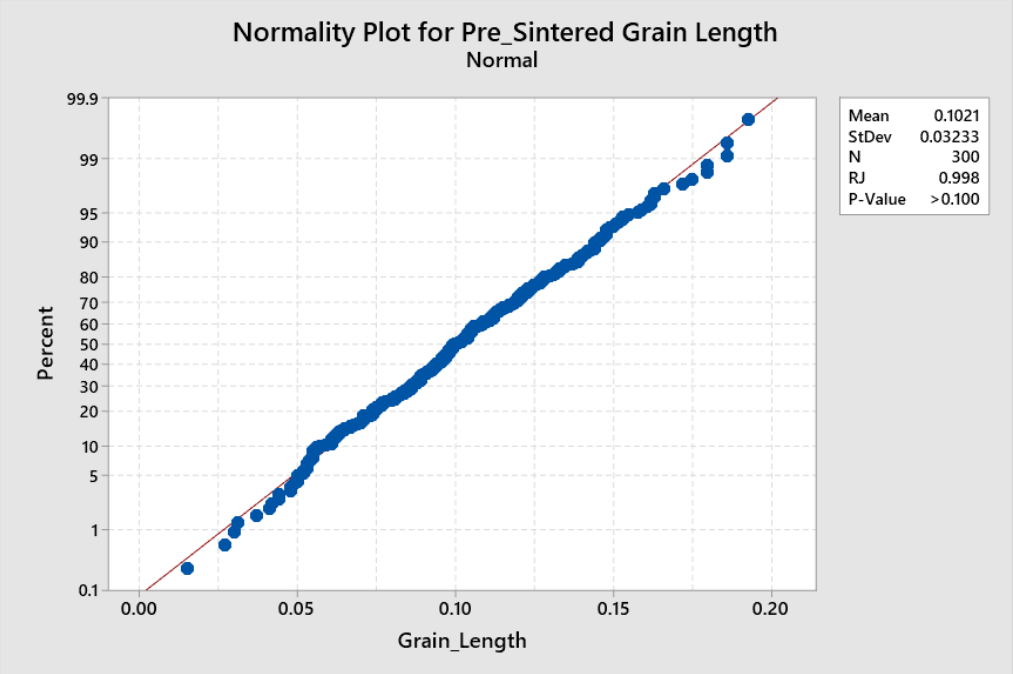

Figure 4.2 Normality plot for grain size measurements of pre-sintered sample (Minitab).

EBSD data reveal an anisotropic crystal structure, as shown in the images below. There is texture, with preference for the (001) plane in the x- and y-directions while the (110) plane in the z-direction occurs less frequently. Anisotropy is a contributing factor in the optical properties of Y-TZP. With the different crystal orientations, light scattering occurs and translucency diminishes (Zhang, 2014).

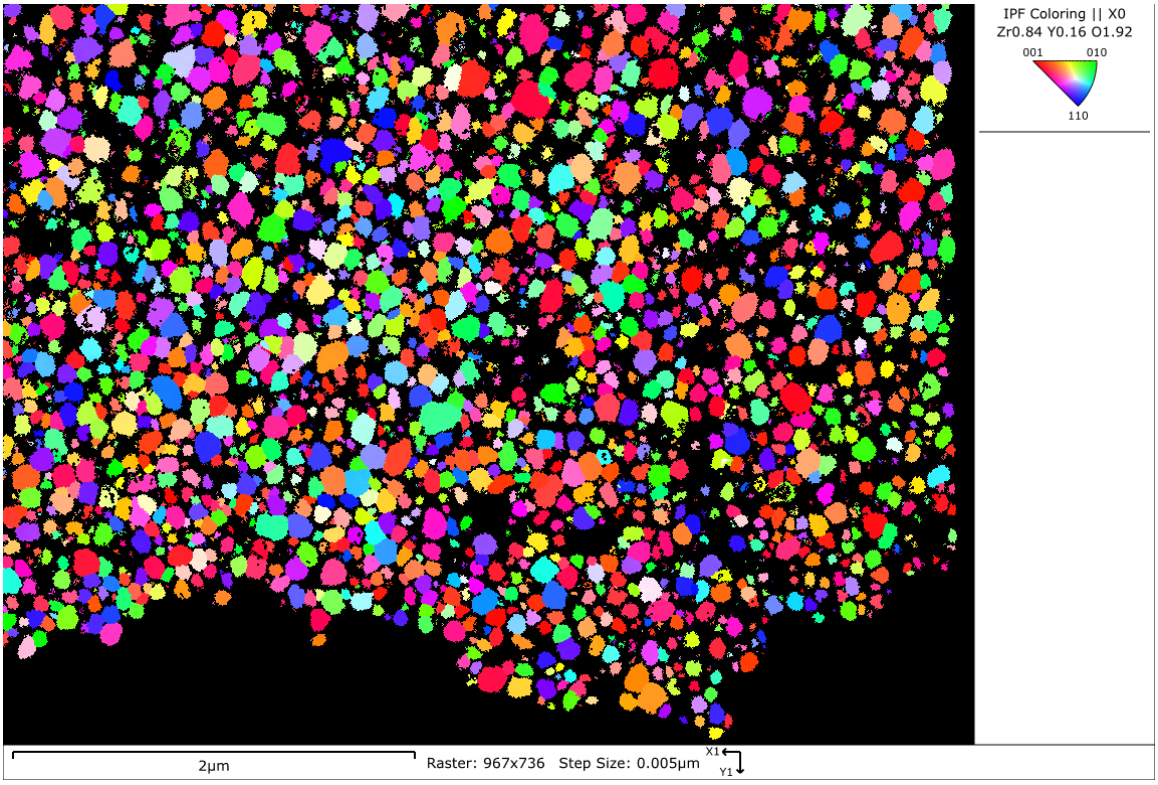

Figure 4.3 Inverse pole figure (x-direction) from EBSD of the pre-sintered material.

EDS results are reported in Table 4.1. The elements match with what Ivoclar Vivadent has shared (Table 4.2), with some additional elements as well. Due to the unsintered state of the ceramic, the layers are not as easily distinguishable.

Table 4.1 EDS results of elemental composition of the pre-sintered sample.

Element	Wt%
Zr	60
O	24
C	14
Y	4.5
Hf	1.5
Fe	0.5
La	0.4
Ca	0.3
Al	0.2
Fe	0.2
Na	0.1

Table 4.2 Elemental composition of IPS e.max ZirCAD Prime (Ivoclar Vivadent).

Material	Percentage
ZrO_2	88.0 – 95.5
Y_2O_3	> 4.5 - ≤ 7.0
HfO_2	≤ 5.0
Al_2O_3	≤ 1.0
Other oxides	≤ 1.5

4.2 Post-Sintered Sample

After sintering, there appears to be complete elimination of pores and the grains are distinguishable from each other as shown in Figure 4.4 below.

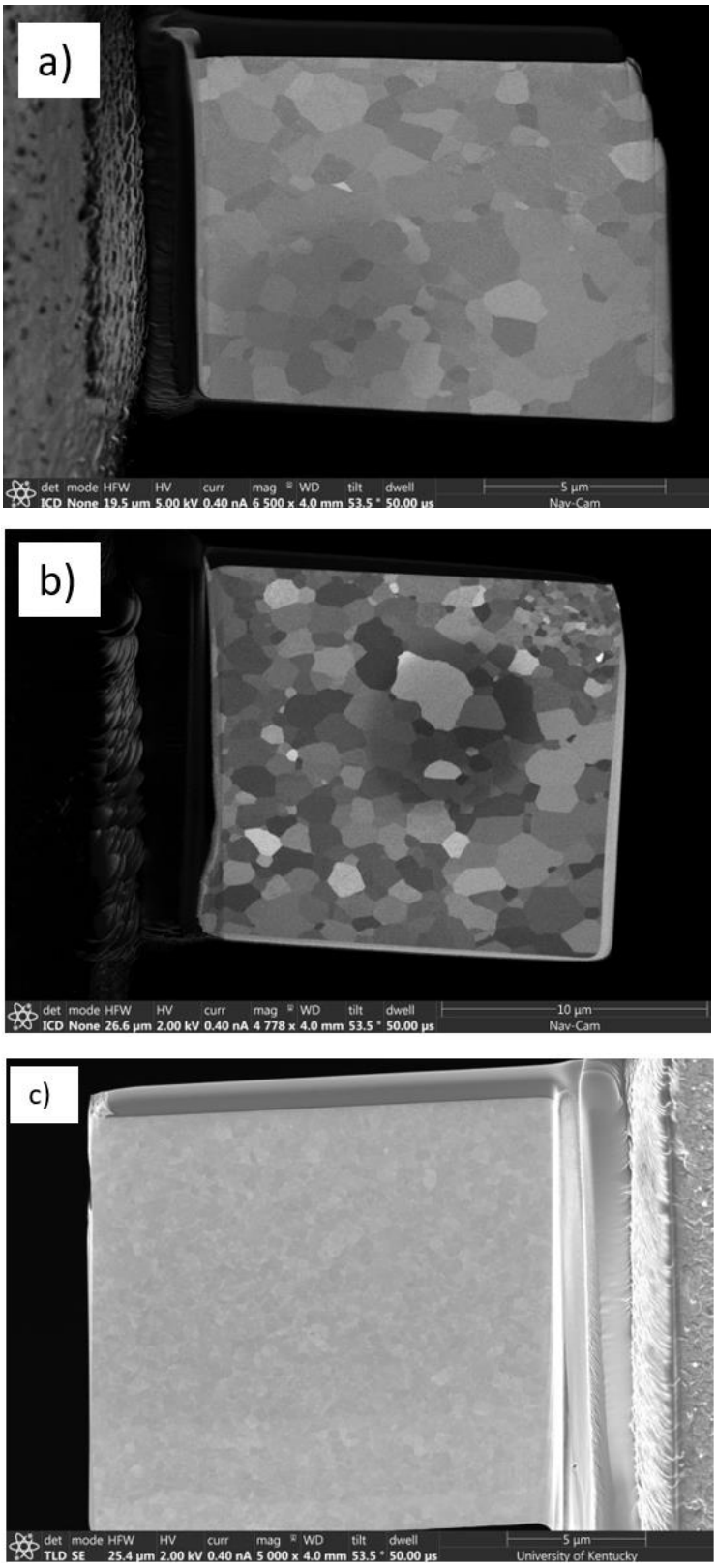

Figure 4.4 SEM lift out images taken after sintering of a) top layer, b) transition layer, and c) the bottom layer.

Grain sizes were measured for each layer and box plots showed unequal variances between the three layers as well as outliers. Since the measurements were taken manually using the ImageJ software, the outliers were removed from the datasets. Histograms of each layer's grain size distribution as well as the Anderson-Darling Normality Test revealed non-normality in the transition layer (Figure 4.5). Johnson transformation was performed to normalize the data from the transition layer. One way ANOVA was conducted to determine whether the means are statistically different, followed by post hoc Tukey test. The average grain size of the bottom layer is significantly different from the top and transition layers (Figure 4.6). Mood's median test was conducted in support of ANOVA to determine if the medians of each layer are different. The differences between the medians of the groups are also found to be statistically different.

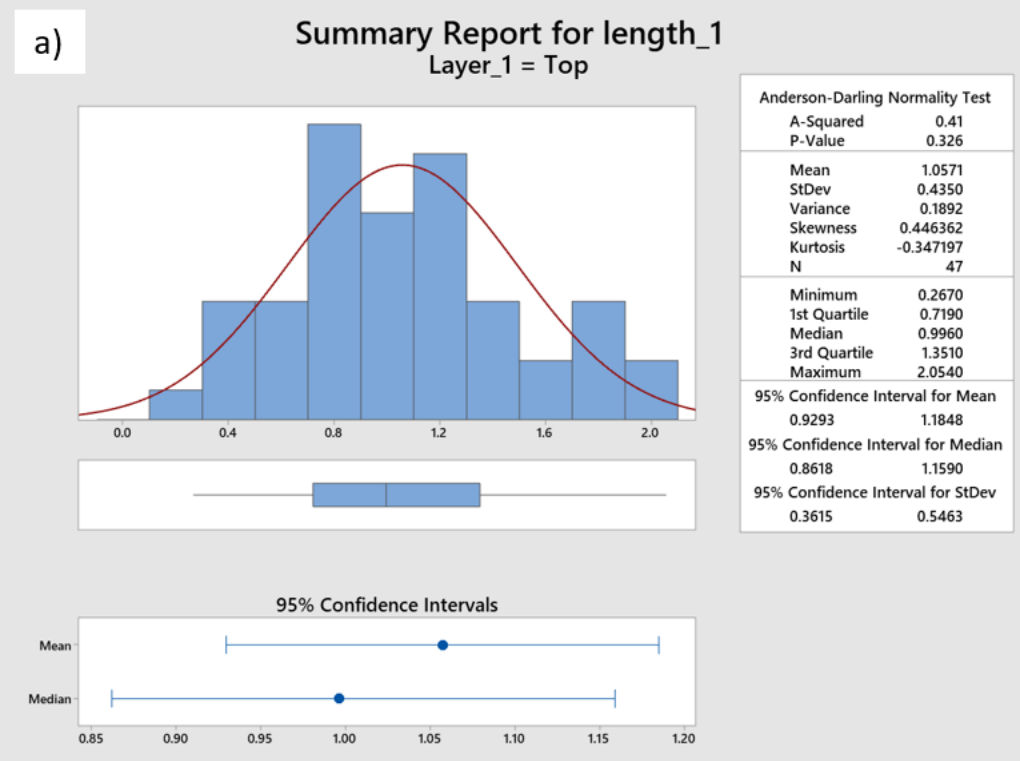

Figure 4.5 Grain size distributions for each of the three layers, a) top, b) transition, and c) bottom, in the sintered sample (Minitab).

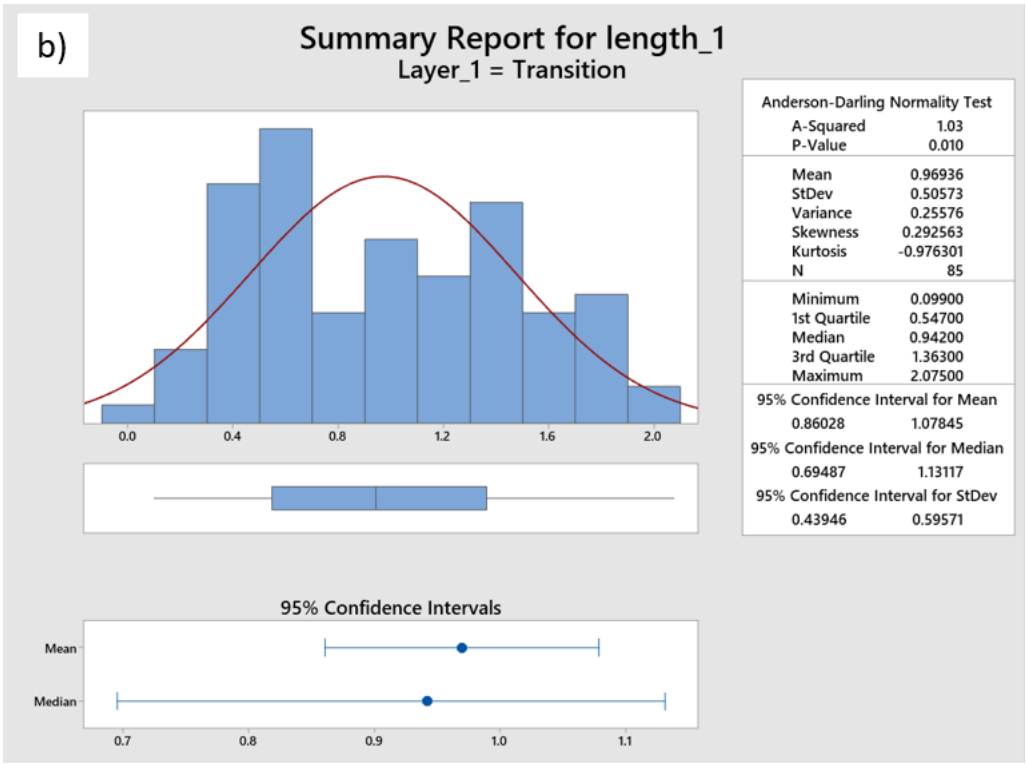

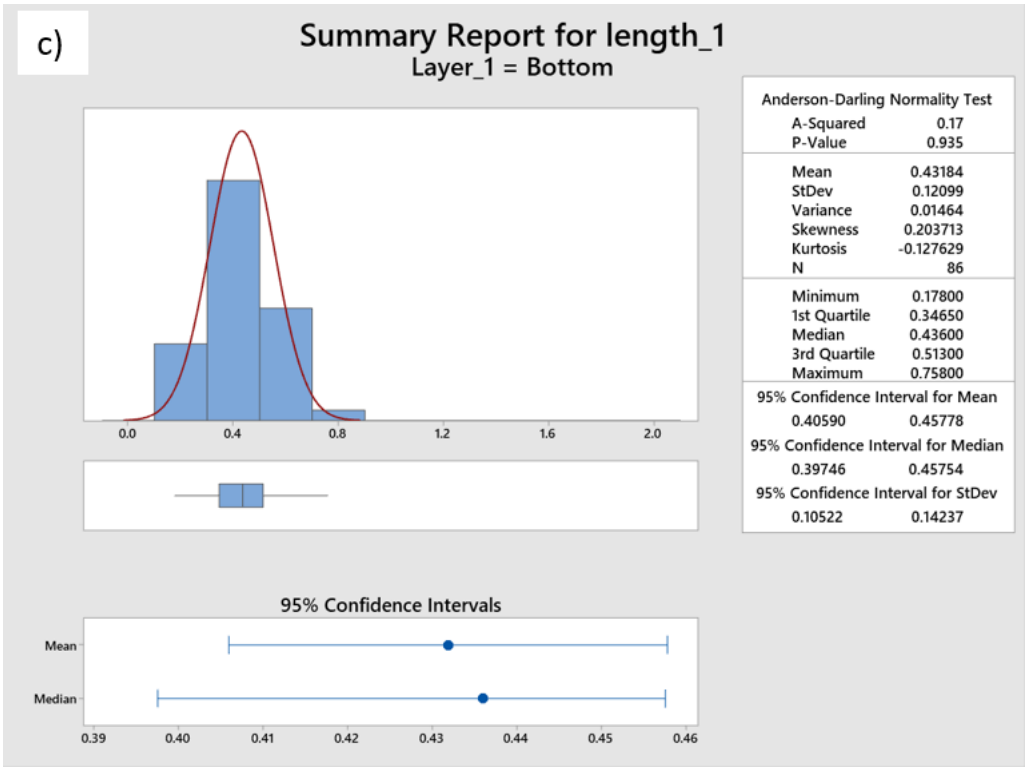

Figure 4.5 Continued.

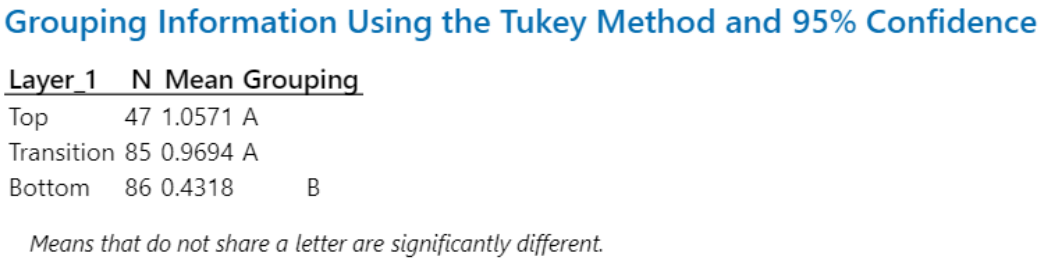

Figure 4.6 Comparison of average grain sizes using the post hoc Tukey test at a significance level of 95% (Minitab).

The average grain sizes and standard deviations of each layer are reported in Table 4.3. There is an increase in grain size from the pre-sintered to post-sintered state. This means that the grains have coalesced, or grain coarsening has occurred. The average grain sizes of the layers decrease going top to bottom. The top layer consists mostly of the cubic structure which is of a larger grain size while the tetragonal phase contributes to the small grain sizes in the bottom layer. The grain distribution varies across the layers as well. The larger distribution in the transition layer can be attributed to the mixture of 3Y-TZP and 5Y-TZP, which is a combination of the large cubic grains and smaller tetragonal grains in varying amounts.

Table 4.3 Average grain size and standard deviation for each layer of the post-sintered sample.

	Mean (um)	Standard Deviation
Top Zone	1.06	0.435
Transition Zone	0.969	0.506
Bottom Zone	0.432	0.121

EBSD results still indicate slight anisotropy after sintering. The preferred orientation is the (001) plane in the x- and y-directions. The (010) plane in the z-direction occurs less frequently.

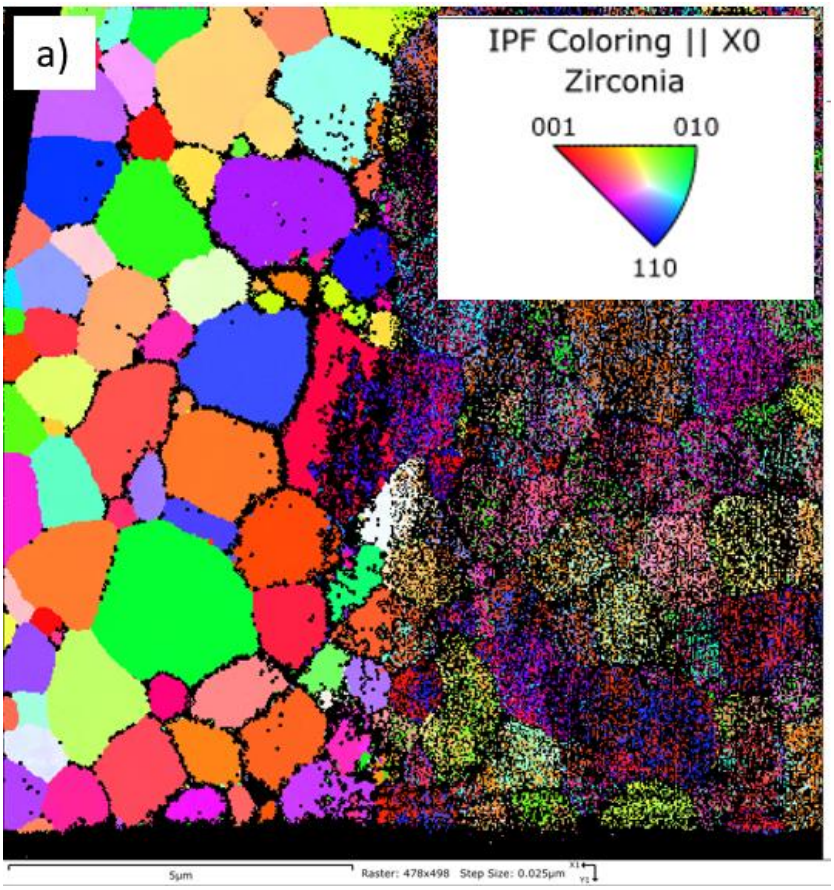

Figure 4.7 Inverse pole figure (x-direction) from EBSD of the sintered layers, a) top, b) transition, and c) bottom.

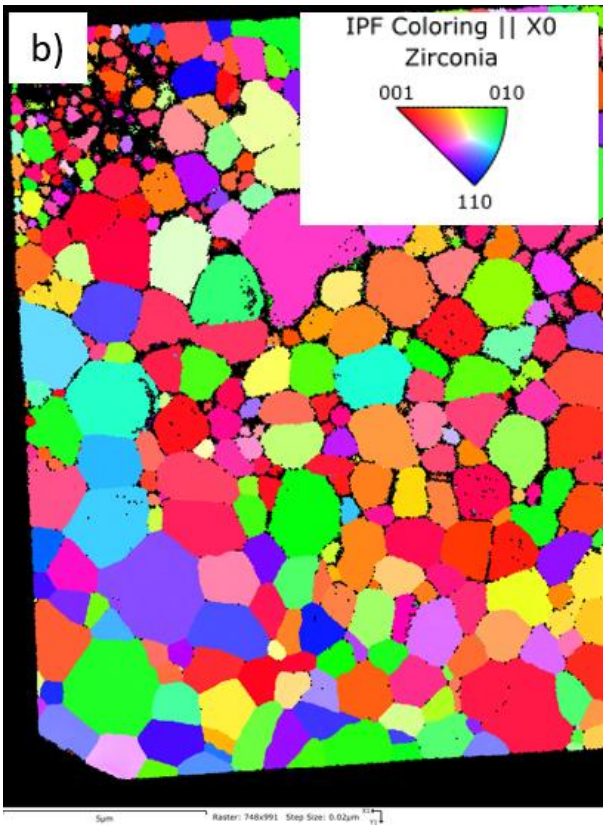

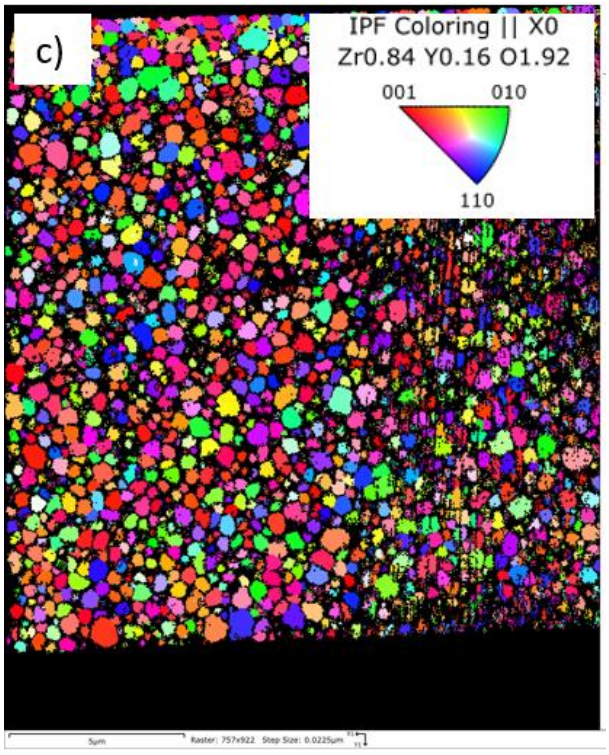

Figure 4.7 Continued

EDS results of the post-sintered sample are listed in Table 4.4. Some elements detected in the pre-sintered state are not found after sintering (Ca, Mg, Na). The most important takeaway is the gradual increase of the yttria content from the bottom to top layer, reflecting the gradient technology of the ZirCAD Prime ceramic (refer to Figure 4.8 below).

Table 4.4 Elemental composition of sintered sample

Element	Wt%
Zr	60
O	19.5
C	20
Y	3-6
Hf	1.5
Fe	0.5
La	0.4
Al	0.2

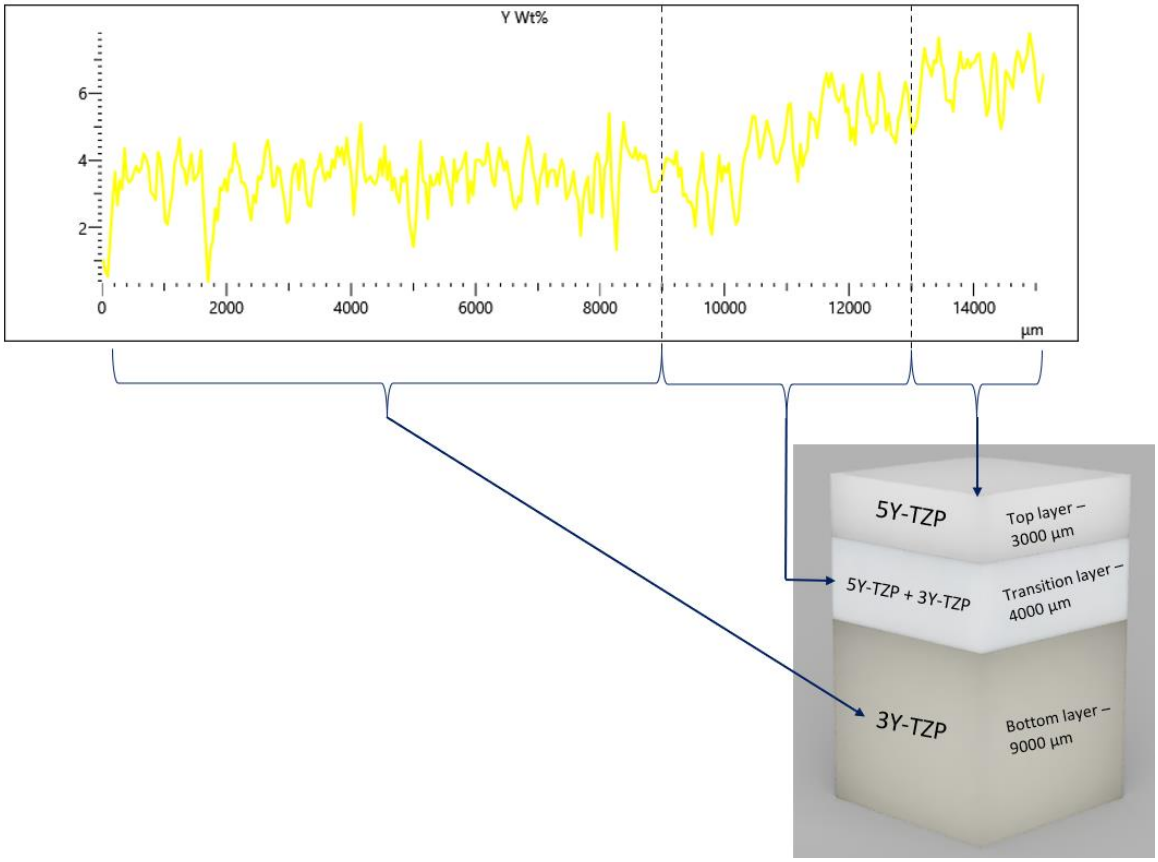

Figure 4.8 Schematic of varying yttria content from EDS over the different layers of the sintered sample.

4.3 Recommendations for Finishing Parameters

Feed rates for dental handpieces are hard to quantify due to user-dependency. Unlike a CNC machine where the movement of the tool is controlled, human motion is variable. But what can be controlled is the tool material and geometry as well as the workpiece, for which there is a better understanding with the grain sizes characterized in this study. Based on these parameters, linear feed rates can be estimated, using the equation below:

$$Linear\ feed\ rate = V_c * f * N$$

where:

- V_c is the spindle speed (in RPM)
- f is critical feed rate (in µm/tooth/revolution)
- N is the number of effective teeth of the grinding tool

The critical (maximum) feed rate considers two average grain diameters as the flaw size (Schoop, 2015). It takes into account the ductile region of the material that must be maintained, so that the brittle zone is not reached and crack formation is minimized. The tool of choice is fine diamond bur for grinding, as it is recommended for both pre-sintered and post-sintered processing by the manufacturer. The diamond bur is assumed to be of fine grit size of 20 µm and diameter of 1.3 mm (Song & Yin, 2010), spinning at 15,000 revolutions per minute, resulting in a cutting speed of 61.3 m/min (Chavali et al., 2015). Table 4.5 below summarizes the different linear feed rates as they pertain to the pre-sintered and post-sintered ZirCAD Prime ceramic.

Table 4.5 Critical feed rates and linear feed rates for ZirCAD Prime, assuming a diamond bur with 20 µm grit size and 1.3 mm diameter.

ZirCAD Prime sample	Avg. grain size (µm)	Critical feed rate (µm/tooth/rev)	Linear feed rate (mm/sec)
Pre-sintered	0.102	0.204	5.3
Post-sintered – top layer	1.06	2.12	54.6
Post-sintered – transition layer	0.969	1.94	49.9
Post-sintered – bottom layer	0.432	0.864	22.2

The calculated linear feed rates are maximum thresholds, beyond which the critical feed rate will be surpassed and brittle fracture may occur. At a cutting speed of 61.3 m/min,

the linear feed rate can be exceeded if a dentist grinds aggressively by applying more force. But when higher cutting speeds are applied, more heat will be generated, causing workpiece to become more ductile. So raising the cutting speed results in an increase in the linear feed rate, allowing a much higher range for the dentist to operate within, before the critical feed rate can be reached. This is in agreement with previous studies. Alao et al. (2016) found that high deformation rates in indentation, which correspond to high cutting speeds in abrasive machining are favorable for material removal in the ductile mode. For sintered 8Y-PSZ, Yoon et al. (2019) observed that higher cutting speeds widened the plastic deformation zone in front of the tool, allowing for an increased ductile cutting length. Therefore, the key recommendation of this study is to use higher cutting speeds to avoid early fracture.

In addition, it may be difficult for dentists to distinguish between the different layers of the restoration once it has been milled and separated from the original disc. To avoid any uncertainties, another recommendation of this study is to use the minimum cutting speed needed for the bottom layer throughout the entire restoration. The bottom layer requires greater cutting speeds due to its smaller grain size. The other two layers are not significantly different from each other, so the minimum cutting speed required for the bottom layer will encompass what is necessary for the top and transition layers.

CHAPTER 5. CONCLUSION

The microstructure of IPS e.max ZirCAD Prime (before and after sintering) was characterized using EDS, EBSD, and SEM. EDS data confirmed the gradient in yttria content over the three layers of the material. EBSD data showed the grain structure and crystallographic orientation, with slight anisotropy. SEM revealed that the three layers were chemically different. Pre-sintered ZirCAD Prime was found to have an average grain size of 0.102 um (SD: 0.032). After sintering, average grain size measurements in the top 5Y-TZP layer, 5Y-TZP + 3Y-TZP transition layer, and bottom 3Y-TZP layer were calculated to be 1.06 um (SD: 0.435), 0.969 um (SD: 0.506), and 0.432 um (SD: 0.121), respectively. The bottom layer was found to be significantly different from the top and transition layers.

Critical feed rates were derived from average grain size measurements. In order to remain in the ductile mode during surface finishing - therefore minimizing brittle fracture and the risk of potential failure of the dental ceramic - dental professionals are recommended to use higher cutting speeds while operating dental handpieces. Also, since the bottom layer has a smaller average grain size that is significantly different from the other two layers, it is recommended that the minimum cutting speed needed for the bottom layer is used throughout the restoration, in case the boundaries between the three layers become unclear to dentists.

CHAPTER 6. FUTURE WORK

Experimental data is necessary to validate the findings of this study. Design of Experiments can help to evaluate the effects of each machining parameter (e.g. tool material, cutting speed, and linear feed rate) on each layer of IPS e.max ZirCAD Prime. There are many grinding and polishing systems available on the market and the effects of higher cutting speeds on tool wear and thermal shock need to be considered.

Additional characterization methods (microstructural, mechanical, optical, thermal, etc.) will help to get a better understanding of the effects of machining parameters on the material. An area of focus would be local tetragonal to monoclinic phase transformation due to grinding and its consequences. Long term studies could be conducted to monitor the aging and degradation.

REFERENCES

Alao, A.-R., Stoll, R., Song, X.-F., Miyazaki, T., Hotta, Y., Shibata, Y., & Yin, L. (2017). Surface quality of yttria-stabilized tetragonal zirconia polycrystal in CAD/CAM milling, sintering, polishing and sandblasting processes. *Journal of the Mechanical Behavior of Biomedical Materials*, 102-116. Retrieved from https://doi.org/10.1016/j.jmbbm.2016.08.021

Ali, S. E., Karthigeyan, S., Deivanai, M., & Mani, R. (2014). Zirconia: Properties and Application - A Review. *Pakistan Oral & Dental Journal, 34*(1).

Arena, A., Prete, F., Rambaldi, E., Bignozzi, M. C., Monaco, C., Di Fiore, A., & Chevalier, J. (2019). Nanostructured Zirconia-Based Ceramics and Composites in Dentistry: A State-of-the-Art Review. *Nanomaterials (Basel)*. doi:10.3390/nano9101393

Armstrong, R. W. (1970). The influence of polycrystal grain size on several mechanical properties of materials. *Metallurgical Transactions*, 1169-1176.

Bifano, T., Dow, T., & Scattergood, R. (1991). Ductile-Regime Grinding: A New Technology for Machining Brittle Materials. *Journal of Engineering for Industry*. doi:10.1115/1.2899676

Chavali, R., Lin, C. P., & Lawson, N. C. (2015). Evaluation of Different Polishing Systems and Speeds for Dental Zirconia. *Journal of Prosthodontics*, 410-418. Retrieved from https://doi.org/10.1111/jopr.12396

Chevalier, J., & Gremillard, L. (2011). Zirconia as a Biomaterial. *Elsevier,* 95-108, ISBN 9780080552941, https://doi.org/10.1016/B978-0-08-055294-1.00017-9.

Choudhary, A., & Paul, S. (2021). Surface generation in high-speed grinding of brittle and tough ceramics. *Ceramics International*. Retrieved from https://doi.org/10.1016/j.ceramint.2021.07.233

Datye, A., & DeLaRiva, A. (2023). Scanning Electron Microscopy (SEM). *Springer Handbook of Advanced Catalyst Characterization*. Retrieved from https://doi.org/10.1007/978-3-031-07125-6_18

Denry, I., & Kelly, J. R. (2008). State of the art of zirconia for dental applications. *Dental Materials*, 299-307.

Dimitriadis, K., Constantinou, M., Moschovas, D., Constantinides, G., & Agathopoulos, S. (2023). Microstructural features, physico-mechanical properties, and wear behavior of dental translucent polychromic multilayer zirconia of hybrid composition prepared by milling technology. *Journal of Esthetic and Restorative Dentistry*, 1-10. doi:10.1111/jerd.13047

Eichler, J., Rodel, J., Eisele, U., & Hoffman, M. (2007). Effect of Grain Size on Mechanical Properties of Submicrometer 3Y-TZP: Fracture Strength and Hydrothermal Degradation. *Journal of American Ceramic Society*. doi:10.1111/j.1551-2916.2007.01643.x

Garvie, R. C., Hannink, R. H., & Pascoe, R. T. (1975). Ceramic steel? *Nature*.

Hodoroaba, V.-D. (2020). Energy-dispersive X-ray spectroscopy (EDS). In V.-D. Hodoroabs, W. E. Unger, & A. G. Shard, *Characterization of Nanoparticles.* Elsevier. Retrieved from https://doi.org/10.1016/B978-0-12-814182-3.00021-3

Inokoshi, M., Liu, H., Yoshihara, K., Yamamoto, M., Tonprasong, W., Benino, Y., . . . Zhang, F. (2023). Layer characteristics in strength-gradient multilayered yttria-stabilized zirconia. *Dental Materials*, 430-441. doi:10.1016/j.dental.2023.03.015

Kisi, E. H., & Howard, C. J. (1998). Crystal Structures of Zirconia Phases and their Inter-Relation. *Key Engineering Materials*, 1-36, doi:10.4028/www.scientific.net/KEM.153-154.1.

Marini, G., Saldanha da Rosa, L., Machado, P. S., Silvestre, F. A., Valandro, L. F., Feitosa, V. P., . . . Bacchi, A. (2023). Fatigue performance analysis of strength-graded zirconia polycrystals for monolithic three-unit implant-supported prostheses. *Journal of the Mechanical Behavior of Biomedical Materials*. Retrieved from https://doi.org/10.1016/j.jmbbm.2023.105736

Mayo, M. J. (1993). Superplasticity of Nanostructured Ceramics. In M. Nastasi, D. M. Parkin, & H. Gleiter, *Mechanical Properties and Deformation Behavior of Materials Having Ultra-Fine Microstructures.* Springer. Retrieved from https://doi.org/10.1007/978-94-011-1765-4_23

Michailova, M., Elsayed, A., Fabel, G., Edelhoff, D., Zylla, I. M., & Stawarczyk, B. (2020). Comparison between novel strength-gradient and color-gradient multilayered zirconia using conventional and high-speed sintering. *Journal of the Mechanical Behavior of Biomedical Materials*, doi: 10.1016/j.jmbbm.2020.103977.

Pace Technologies. (n.d.). *Zirconia Engineering Ceramic*. Retrieved from https://www.metallographic.com/Metallographic-Preparation-Procedures/Zirconia-ceramic.htm

Pelleg, J. (2014). *Mechanical Properties of Ceramics.* Springer Cham.

Piconi, C., & Maccauro, G. (1999). Zirconia as a ceramic biomaterial. *Biomaterials*, 1-25,. doi:10.1016/s0142-9612(98)00010-6

Rosentritt, M., Preis, V., Schmid, A., & Strasser, T. (2020). Multilayer zirconia: Influence of positioning within blank and sintering conditions on the in vitro

performance of 3-unit fixed partial dentures. *The Journal of Prosthetic Dentistry*. doi:https://doi.org/10.1016/j.prosdent.2020.11.009

Sakaguchi, R., Powers, J., & Ferracane, J. (2019). *Craig's Restorative Dental Materials.* Elsevier, Inc. Retrieved from https://doi.org/10.1016/C2015-0-01767-1.

Schey, J. A. (1999). *Introduction to Manufacturing Processes.* Tata McGraw Hill India.

Singh, A., Solanki, D., Sencha, R., Singh, R. K., & Mote, R. G. (2020). Study and characterization of the ductile-brittle transition zone in sintered zirconia. *Journal of Manufacturing Processes*, 749-762.

Schoop, Julius M., "Engineered Surface Properties of Porous Tungsten from Cryogenic Machining" (2015). Theses and Dissertations--Chemical and Materials Engineering. 49. https://uknowledge.uky.edu/cme_etds/49

Singhal, S. (2020, January 17). *IPS e.max ZirCAD Prime*. Retrieved from Aesthetic Dentistry: https://adentmag.com/ips-e-max-zircad-prime/

Skorulska, A., Piszko, P., Rybak, Z., Szymonowicz, M., & Dobrzyński, M. (2021). Review on Polymer, Ceramic and Composite Materials for CAD/CAM Indirect Restorations in Dentistry-Application, Mechanical Characteristics and Comparison. *Materials (Basel)*. doi:10.3390/ma14071592

Soleimani, F., Jalali, H., Mostafavi, A. S., Zeighami, S., & Memarian, M. (2020). Retention and Clinical Performance of Zirconia Crowns: A Comprehensive Review. *International Journal of Dentistry*. Retrieved from https://doi.org/10.1155/2020/8846534

Song, X.-F., & Yin, L. (2010). The Quantitative Effect of Diamond Grit Size on the Subsurface Damage Induced in Dental Adjustment of Porcelain Surfaces. *Journal of Engineering in Medicine*. doi:10.1243/09544119JEIM737

Stawarczyk, B., Keul, C., Eichberger, M., Figge, D., Edelhoff, D., & Lümkemann, N. (2017). Three generations of zirconia: From veneered to monolithic. *Quintessence Int*, 369-380. doi:10.3290/j.qi.a38057. PMID: 28396886

Strasser, T., Wertz, M., Koenig, A., Koetzsch, T., & Rosentritt, M. (2023). Microstructure, composition, and flexural strength of different layers within zirconia materials with strength gradient. *Dental Materials*. Retrieved from https://doi.org/10.1016/j.dental.2023.03.012i

Sun, L., Yang, S., Yang, L., Zhao, P., Wu, P., & Jiang, Z. (2015). A new model of grinding forces prediction for machining brittle and hard materials. *Procedia CIRP*, 192-197.

Trunec, M. (2008). Effect of Grain Size on Mechanical Properties of 3Y-TZP Ceramics. *Ceramics - Silikaty*, 165-171.

Vardhaman, S., Borba, M., Kaizer, M. R., Kim, D. K., & Zhang, Y. (2020). Wear behavior and microstructural characterization of translucent multilayer zirconia. *Dental Materials*. doi:10.1016/j. dental.2020.08.015

Wilkinson, A. J., & Britton, T. B. (2012). Strains, planes, and EBSD in materials science. *Materials Today*. Retrieved from https://doi.org/10.1016/S1369-7021(12)70163-3

Winter, A., Schurig, A., Odenthal, A., & Schmitter, M. (2022). Impact of different layers within a blank on mechanical properties of multi-layered zirconia ceramics before and after thermal aging. *Dental Materials*. Retrieved from https://doi.org/10.1016/j.dental.2022.03.009

Yang, M., Li, C., Zhang, Y., Jia, D., Li, R., Hou, Y., & Cao, H. (2019). Effect of friction coefficient on chip thickness models in ductile-regime grinding of zirconia ceramics. *The International Journal of Advanced Manufacturing Technology*. Retrieved from https://doi.org/10.1007/s00170-019-03367-0

Yang, X. Z., Bai, Q., Zheng, M., & Tang, J. (2020). Grain size influence on chip formation in high-speed machining of pure iron. *The International Journal of Advanced Manufacturing Technology*. Retrieved from https://doi.org/10.1007/s00170-020-05512-6

Yoon, H.-S., Lee, S., & Min, S. (2018). Investigation of ductile-brittle transition in machining of yttrium-stabilized zirconia. *Procedia Manufacturing*. doi:10.1016/j.promfg.2018.07.052

Zhang, F., Van Meerbeek, B., & Vleugels, J. (2020). Importance of tetragonal phase in high-translucent partially stabilized zirconia for dental restorations. *Dental Materials*, 491-500. doi:10.1016/j.dental.2020.01.017

Zhang, Y. (2014). Making yttria-stabilized tetragonal zirconia translucent. *Dental Materials*. doi:10.1016/j.dental.2014.08.375

Zhang, Y., & Lawn, B. R. (2019). Evaluating dental zirconia. *Dental Materials*, 15-23. doi:10.1016/j.dental.2018.08.291

VITA

Angani Vigneswaran

Education

Bachelor of Science in Materials Science and Engineering

University of California, Davis | June 2020

Professional Experience

Manufacturing Engineer

SMART Modular Technologies | October 2021 – Present

Engineering Associate (Process Development)

Tactus Technology | October 2020 – August 2021

Engineering Student Assistant

Caltrans Office of Pavement Management | July 2019 – October 2020